

The uncertainty in Galactic parameters

Paul J. McMillan^{*}, and James J. Binney

Rudolf Peierls Centre for Theoretical Physics, 1 Keble Road, Oxford, OX1 3NP, UK

28 October 2018

ABSTRACT

We reanalyse the measurements of parallax, proper motion, and line-of-sight velocity for 18 masers in high mass star-forming regions presented by Reid et al. (2009). We use a likelihood analysis to investigate the distance of the Sun from the Galactic centre, R_0 , the rotational speed of the local standard of rest, v_0 , and the peculiar velocity of the Sun, \mathbf{v}_\odot , for various models of the rotation curve, and models which allow for a typical peculiar motion of the high mass star-forming regions.

We find that these data are best fit by models with non-standard values for \mathbf{v}_\odot or a net peculiar motion of the high mass star-forming regions. We argue that a correction to \mathbf{v}_\odot is much more likely, and that these data support the conclusion of Binney (2009) that V_\odot should be revised upwards from 5.2 km s^{-1} to 11 km s^{-1} . We find that the values of R_0 and v_0 that we determine are heavily dependent on the model we use for the rotation curve, with model-dependent estimates of R_0 ranging from $6.7 \pm 0.5 \text{ kpc}$ to $8.9 \pm 0.9 \text{ kpc}$, and those of v_0 ranging from $200 \pm 20 \text{ km s}^{-1}$ to $279 \pm 33 \text{ km s}^{-1}$. We argue that these data cannot be thought of as implying any particular values of R_0 or v_0 . However, we find that v_0/R_0 is better constrained, lying in the range $29.9 - 31.6 \text{ km s}^{-1} \text{ kpc}^{-1}$ for all models but one.

Key words: Galaxy: fundamental parameters – methods: statistical – Galaxy: kinematics and dynamics

1 INTRODUCTION

The fundamental parameters that define the Solar position and velocity within the Galaxy remain uncertain to a remarkable degree. The major remaining uncertainty is that in the distance from the Sun to the Galactic centre, R_0 . The most recent results from studies of stellar orbits in the Galactic centre (Ghez et al. 2008; Gillessen et al. 2009) give values of $R_0 = (8.4 \pm 0.4) \text{ kpc}$ and $R_0 = (8.33 \pm 0.35) \text{ kpc}$ respectively. These can be compared to the earlier estimate in the review by Reid (1993) of $R_0 = (8.0 \pm 0.5) \text{ kpc}$.

The total velocity of the Sun about the Galactic centre is the sum of the velocity of the local standard of rest (LSR), v_0 , and the peculiar motion of the Sun with respect to the LSR in the same direction, V_\odot . This total velocity can be determined using the apparent proper motion of Sgr A^{*}, μ_{A^*} , since it is expected to be moving with a peculiar velocity less than $\sim 1 \text{ km s}^{-1}$ at the Galactic Centre. This constraint on the peculiar motion of Sgr A^{*} is justified by the observation that the velocity of Sgr A^{*} perpendicular to the plane is consistent with zero, with uncertainties $\sim 1 \text{ km s}^{-1}$ (Reid & Brunthaler 2004), and because this motion is thought to be due to stochastic forces from

discrete interactions with individual stars, so the velocity in the plane should be similar to that perpendicular to it (Chatterjee, Hernquist, & Loeb 2002). Reid & Brunthaler (2004) found $\mu_{A^*} = (6.379 \pm 0.024) \text{ mas yr}^{-1}$, which corresponds to $(v_0 + V_\odot)/R_0 = (30.2 \pm 0.2) \text{ km s}^{-1} \text{ kpc}^{-1}$, or a velocity about the Galactic centre (using the Ghez et al. result for R_0) of $v_0 + V_\odot = (252 \pm 11) \text{ km s}^{-1}$, where by far the dominant uncertainty comes from the value of R_0 . Analysis of the GD-1 stellar stream (Koposov, Rix, & Hogg 2009) has recently been used to suggest a significantly lower value, $v_0 = 221_{-20}^{+16} \text{ km s}^{-1}$.

The velocity of the Sun with respect to the local standard of rest, \mathbf{v}_\odot , is often assumed to be well known and constrained to within $\sim 0.5 \text{ km s}^{-1}$ because of the analysis of the dynamics of nearby stars conducted by Dehnen & Binney (1998, henceforth DB98), and again more recently, using identical techniques, by Aumer & Binney (2009). DB98 found

$$\mathbf{v}_\odot \equiv (U_\odot, V_\odot, W_\odot) \\ = (10.00 \pm 0.36, 5.25 \pm 0.62, 7.17 \pm 0.38) \text{ km s}^{-1}, \quad (1)$$

which has been widely accepted and used. However Binney (2009, henceforth B09) suggests that the value for V_\odot determined in these papers may be an underestimate by $\sim 6 \text{ km s}^{-1}$. This is because the analysis by DB98 uses Stromberg’s equation, which is derived under the assump-

^{*} E-mail: p.mcmillan1@physics.ox.ac.uk

tion that the Galactic potential is axisymmetric, and extrapolates to zero velocity dispersion. In practice, the Galactic potential is not axisymmetric, and the smaller the velocity dispersion of a population, the more it is affected by departures from axisymmetry. B09 uses a more global approach, ensuring that more emphasis is placed on stellar populations with high velocity dispersions, which one would expect to be less affected by the non-axisymmetry of the Galactic potential.

Reid et al. (2009) brought together observations of masers seen in high mass star-forming regions (HMSFRs) in the Milky Way. They used simple statistical tools in an effort to determine the values of R_0 and v_0 , using the DB98 value of \mathbf{v}_\odot , initially under the assumption that the HMSFRs were moving on circular orbits in a flat rotation curve, for which they offer best-fitting parameters $R_0 = (8.24 \pm 0.55)$ kpc and $v_0 = (265 \pm 26)$ km s $^{-1}$, but with a high χ^2 value.

In addition they considered a model in which the HMSFRs were moving with a characteristic velocity with respect to their local circular velocity. They found that they achieved a significantly improved fit to their data using this model with a peculiar velocity ~ 15 km s $^{-1}$ in the opposite direction to rotation. This fit yielded $R_0 = (8.40 \pm 0.36)$ kpc and $v_0 = (254 \pm 16)$ km s $^{-1}$. They briefly considered a model in which the value of \mathbf{v}_\odot was allowed to vary, finding an acceptable fit with $\mathbf{v}_\odot = (9, 20, 10)$ km s $^{-1}$. However, believing the DB98 result to be “well determined” they did not pursue the matter further.

In this paper we re-examine the data described in Reid et al. (2009), and conduct a likelihood analysis for various models of the velocity distribution of the maser sources. This enables us to exploit these data more thoroughly. We also consider the implications of the results from B09 on the interpretation of these data. In Section 2 we explain what the data consist of, describe our models and our statistical technique; in Section 3 we give the raw results and examine their significance. We discuss the implications of these results in Section 4.

2 METHODS

2.1 The data

These data, as given in Table 1 of Reid et al. (2009), consist of measurements for 18 masers of: Galactic coordinates (l_i, b_i), which we can assume to be exact; parallaxes π_i ; proper motions $\mu_{x,i}$ and $\mu_{y,i}$; line-of-sight velocities $v_{\text{LSR},i}$. For each quantity Reid et al. give an error and we assume that this error together with the measured value of the quantity defines a Gaussian probability distribution for the true value of the quantity. For the proper motions μ_x and μ_y we shall use the more conventional notation μ_α and μ_δ . The line-of-sight velocity v_{LSR} is relative to an obsolete estimate of the LSR. Fortunately the underlying heliocentric line-of-sight velocity v_r can be recovered from v_{LSR} without impact on the associated uncertainty (Reid et al. 2009, Appendix).

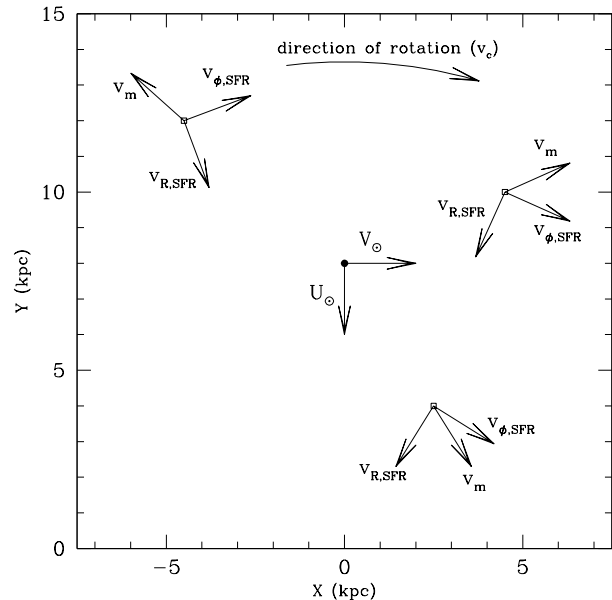


Figure 1. Diagram showing a pole-on view of the Galaxy illustrating the various peculiar velocities we consider (e.g. equation 4). This therefore only shows the in plane components. The Sun (represented by a solid circle) is placed at (0, 8) kpc, and components of its velocity \mathbf{v}_\odot are indicated. Three points (empty squares) are plotted to represent masers, and the directions of the components of any systematic offset from circular velocity in each case (\mathbf{v}_{SFR}) are shown, as is the peculiar velocity due to any bias in the observed radial velocity, v_m . This diagram is purely illustrative and does not show any real data.

2.2 Our models

The motion of both the Sun and the masers is dominated by circular motion around the Galactic centre with velocity

$$-v_c(R)\mathbf{e}_\phi, \quad (2)$$

where $v_c(R) > 0$ and the minus sign reflects the fact that the Galaxy rotates clockwise in our coordinate system. We explore three forms for $v_c(R)$

- A flat rotation curve, $v_c(R) = v_0$, with v_0 being a (positive) free parameter.
- A power-law rotation curve $v_c(R) = v_0(R/R_0)^\alpha$, with v_0 , R_0 and α being free parameters.
- A rotation curve corresponding to that given by the Galactic potential Model I in §2.7 of Binney & Tremaine (2008, henceforth GDII), linearly scaled to variable values of R_0 and v_0 .

In each case, we take the parameters of $v_c(R)$ to have uniform prior probability distributions. This choice ensures that we determine what *these* data tell us, without prejudice.

The velocity of a maser can be expected to differ from the local circular speed. We separate this difference into a random component and (in some cases) two systematic components. Like Reid et al. (2009), we consider the possibility that the velocity of HMSFRs has a systematic offset from the circular velocity, \mathbf{v}_{SFR} . We also consider the possibility that the expansion of the shell within which a maser occurs will

displace the maser's velocity from that of the star, and if we are biased towards seeing masers on the near side of that shell, we will see a bias in radial velocity. We represent this as an average peculiar motion $v_m \mathbf{e}_*$, where \mathbf{e}_* is the unit vector from the Sun to the maser. We assume that the random component of the maser velocities has a Gaussian distribution of dispersion Δ_v . In total we take the probability distribution of the velocities of masers to be

$$p(\mathbf{v}) d^3\mathbf{v} = \frac{d^3\mathbf{v}}{(2\pi\Delta_v^2)^{3/2}} \exp\left(-\frac{|\mathbf{v} - \bar{\mathbf{v}}|^2}{2\Delta_v^2}\right), \quad (3)$$

where

$$\bar{\mathbf{v}} = -v_c(R)\mathbf{e}_\phi - \mathbf{v}_{\text{SFR}} + v_m \mathbf{e}_*. \quad (4)$$

Notice that positive values of $v_{\phi, \text{SFR}}$ imply that the masing stars lead Galactic rotation, and that motion of the masers towards us will be reflected in negative values of v_m . In most cases we fix both $\mathbf{v}_{\text{SFR}} = 0$ and $v_m = 0$. The various velocities are illustrated in Fig. 1.

We sometimes take the Sun's motion with respect to the LSR, \mathbf{v}_\odot , to be specified, and sometimes we fit it to the data.

For given values of l_i , b_i , the heliocentric distance s_i , and R_0 , we deduce the probability distributions in proper motion and line-of-sight velocity given the above probability distribution of the velocity (eq. 3). Since our focus is on the Galaxy's parameters, we marginalise over the s_i . We do this under the assumption that the probability distribution of the s_i is that implied by the assumption of Gaussian errors in the parallaxes.

2.3 Statistical analysis

2.3.1 Likelihood function

In order to determine the best-fitting model parameters, we maximise the likelihood function. This is

$$\mathcal{L}(\boldsymbol{\theta}) \propto \prod_i \int ds_i p(\text{data} | \boldsymbol{\theta}), \quad (5)$$

where $p(\text{data} | \boldsymbol{\theta})$ is the conditional probability of the i th observation, given the model with parameters

$$\boldsymbol{\theta} \equiv (v_0, R_0, \alpha, \mathbf{v}_\odot, \Delta_v, s_i, \dots). \quad (6)$$

For each distance s_i , the model provides a multivariate Gaussian probability distribution in $v_{r,i}$, $\mu_{\alpha,i}$ and $\mu_{\delta,i}$. The data also provide a multivariate Gaussian distribution for the underlying values of these variables. We obtain $p(\text{data} | \boldsymbol{\theta})$ by integrating the product of these two Gaussian distributions over all three variables.

The likelihood function defines the a posteriori probability distribution of the model parameters $\boldsymbol{\theta}$. We use a Metropolis algorithm (Metropolis et al. 1953) to identify the peak in this probability distribution, and to characterise its width around the most probable model. The Metropolis algorithm is a Markov Chain Monte Carlo method for drawing a representative sample from a probability distribution, such as the likelihood function. We start with some choice for the parameters $\boldsymbol{\theta}$, and calculate the associated likelihood $\mathcal{L}(\boldsymbol{\theta})$. We then

- (i) choose a trial parameter set $\boldsymbol{\theta}'$ by moving from $\boldsymbol{\theta}$ in

all directions in parameter space, by an amount chosen at random (from a Gaussian distribution);

- (ii) determine $\mathcal{L}(\boldsymbol{\theta}')$;

(iii) choose a random variable r from a uniform distribution in the range $[0,1]$;

(iv) if $\mathcal{L}(\boldsymbol{\theta}')/\mathcal{L}(\boldsymbol{\theta}) > r$, accept the trial parameter set, and set $\boldsymbol{\theta} = \boldsymbol{\theta}'$. Otherwise do not accept it.

- (v) Return to step (i).

The first few values of $\boldsymbol{\theta}$ are ignored as ‘‘burn-in’’, which helps to remove the dependence on the initial value of $\boldsymbol{\theta}$. We repeat the procedure until the chain of $\boldsymbol{\theta}$ values constitutes a fair sample of the probability distribution – we establish that the burn-in period is sufficiently long by comparing chains that have different starting $\boldsymbol{\theta}$ (e.g. Gelman & Rubin 1992).

2.3.2 Bayesian evidence

In addition to comparing models that differ only in the values taken by a given set of parameters, we have to assess the value of adding a parameter to a model. Adding a parameter is guaranteed to increase the maximum likelihood achievable for given data, but is that increase statistically significant or just the consequence of an enhanced ability to fit noise? The Bayesian methodology for making such assessments is now well established and described by Heavens (2009), for example.

One calculates the ‘‘evidence’’ for the model under different priors for whatever parameters are either fixed a priori or varied. The evidence is the total probability of the data after integrating over all parameters:

$$p(\text{data} | \text{Model}) = \int d^n \boldsymbol{\theta} p(\text{data} | \boldsymbol{\theta}, \text{Model}) p(\boldsymbol{\theta} | \text{Model}). \quad (7)$$

Here $p(\boldsymbol{\theta} | \text{Model})$ is the prior on the parameters. For a parameter θ_i that is varied, we take the prior to be uniform within a range of width $\Delta\theta_i$ that is large enough to encompass any plausible value of θ_i (so $p(\theta_i | \text{Model}) d\theta_i = d\theta_i / \Delta\theta_i$ over this range). The priors on parameters that are always varied play little role because we are interested the ratio of the evidence when a parameter θ_n is fixed to when it is varied. When θ_n is fixed, its prior is a delta function at the chosen value, so the ratio of the evidences when θ_n is fixed to when it is varied is

$$\frac{p(\text{data} | \text{Model}, \theta_n \text{ fixed})}{p(\text{data} | \text{Model})} = \frac{\int d^{n-1} \boldsymbol{\theta} p(\text{data} | \boldsymbol{\theta}, \text{Model})}{\int d^n \boldsymbol{\theta} p(\text{data} | \boldsymbol{\theta}, \text{Model})} \Delta\theta_n, \quad (8)$$

where upper integral excludes θ_n and the lower one includes it.

By Bayes theorem the ratio of the a posteriori probabilities of the model when θ_n is fixed to when it is varied is the ratio of the corresponding evidences times the ratios of the prior on θ_n being fixed to that on it being variable. We take this second factor to be unity, so the a posteriori probabilities of the models is simply the ratio of the evidences.

The integration over the space of parameters that is required to calculate the evidence is exceedingly costly if done by brute force. We approximate it by assuming that in the vicinity of its peak, $p(\text{data} | \boldsymbol{\theta}, \text{model})$ can be approximated by a Gaussian $p \propto \exp(-\boldsymbol{\theta}^T \cdot K \cdot \boldsymbol{\theta})$, where K is a matrix whose eigenvectors and eigenvalues can be estimated from

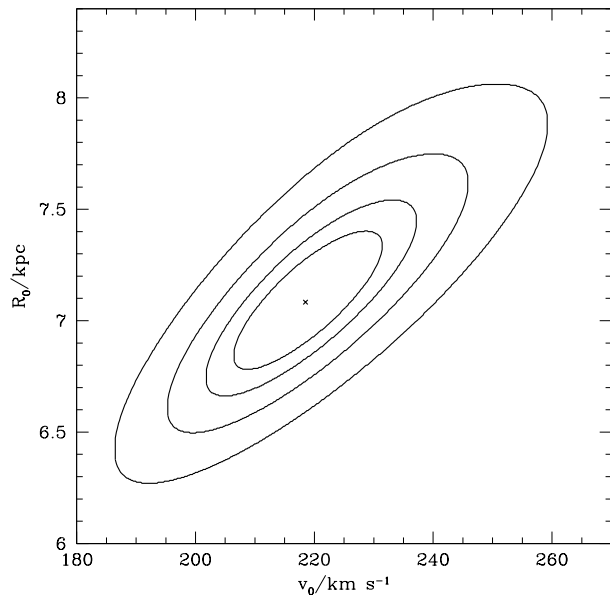


Figure 2. Plot showing contours of the Likelihood function (marginalised over Δv) for a model with the GDII rotation curve, and the DB98 \mathbf{v}_\odot . There is clearly a strong correlation between the values found for v_0 and R_0 . Contours are drawn at likelihood differing from the maximum likelihood $\Delta\mathcal{L} = 0.25, 0.5, 1, 2$.

the output of the Metropolis algorithm. With this approximation, the integral over parameters becomes analytic.

The Metropolis algorithm yields a set of points in parameter space which sample $p(\text{data}|\text{Model})$. Principal component analysis of this sample yields the eigenvectors and eigenvalues of K .

3 RESULTS

We first investigate models in which the masers are at rest with respect to their host stars (i.e., $v_m = 0$).

Table 1 gives the peak likelihoods of our models, as well as the best-fitting parameters and the corresponding uncertainties. The best-fitting value of v_0 varies in the range (200 – 279) km s^{-1} , and that of R_0 between 6.7 and 8.9 kpc. As Fig. 2 illustrates, v_0 and R_0 are strongly correlated with the result that v_0/R_0 is confined to the relatively narrow range 29.9 – 31.6 $\text{km s}^{-1} \text{ kpc}^{-1}$.

When \mathbf{v}_\odot is a free parameter, the best-fitting values of U_\odot and W_\odot are close to the DB98 values, and essentially independent of the form of the rotation curve, whereas V_\odot varies in the range 16.5 – 19.5 km s^{-1} . Similarly, when \mathbf{v}_\odot is fixed at the DB98 value and \mathbf{v}_{SFR} is a free parameter, only $v_{\phi, \text{SFR}}$ takes a value that is far removed from that which one would naively expect – it moves in the range –11.0 to –14.8 km s^{-1} . Thus the data suggest either that the Sun is circulating significantly faster than the circular speed, or that the HMSFR have an appreciable rotational lag.

The fits are almost perfectly degenerate between \mathbf{v}_\odot and \mathbf{v}_{SFR} : they constrain only the difference between these velocities. However, we shall argue in Section 4 that significantly non-zero values of \mathbf{v}_{SFR} are physically implausible,

so here we focus on what can be inferred about \mathbf{v}_\odot given $\mathbf{v}_{\text{SFR}} = 0$. In view of the degeneracy between \mathbf{v}_\odot and \mathbf{v}_{SFR} we do not report results obtained when both \mathbf{v}_\odot and \mathbf{v}_{SFR} are varied.

When $\mathbf{v}_{\text{SFR}} = 0$, the peak likelihood is higher when \mathbf{v}_\odot is fixed to the B09 value than when it is fixed to the DB98 value. To assess the significance of this increase in likelihood, we calculate the ratio of the evidences for the two models as described in Section 2.3.2

$$\frac{p(\text{DB98}|\text{data})}{p(\text{B09}|\text{data})} \simeq \begin{cases} 2 \times 10^{-4} & \text{for } \alpha = 0 \\ 1 \times 10^{-4} & \alpha \text{ variable} \\ 4 \times 10^{-4} & \text{GDII.} \end{cases} \quad (9)$$

Thus regardless of the adopted rotation curve, the data strongly favour upward revision of V_\odot from 5.2 km s^{-1} to 11 km s^{-1} .

When \mathbf{v}_\odot is a free parameter, the peak likelihood of the B09 model is surpassed at yet larger values of V_\odot . To determine whether the increase in likelihood that occurs when \mathbf{v}_\odot is set free from the B09 value, we again calculate the relevant ratio of the evidences. Since the two models now differ in whether \mathbf{v}_\odot is fixed or free, the priors on the components of \mathbf{v}_\odot now become relevant (cf eq. 8). We have adopted $\Delta U_\odot = \Delta V_\odot = \Delta W_\odot = 100 \text{ km s}^{-1}$. With these values we have

$$\frac{p(\text{B09}|\text{data})}{p(\mathbf{v}_\odot \text{ free}|\text{data})} \simeq \begin{cases} 5 & \text{for } \alpha = 0 \\ 0.6 & \alpha \text{ variable} \\ 40 & \text{GDII.} \end{cases} \quad (10)$$

Therefore under these assumptions the increase in likelihood attained on setting \mathbf{v}_\odot free from the B09 value is not statistically significant. The ratio of evidences for the case when \mathbf{v}_\odot is set to the DB98 value or is set free is

$$\frac{p(\text{DB98}|\text{data})}{p(\mathbf{v}_\odot \text{ free}|\text{data})} \simeq \begin{cases} 8 \times 10^{-4} & \text{for } \alpha = 0 \\ 7 \times 10^{-5} & \alpha \text{ variable} \\ 0.01 & \text{GDII.} \end{cases} \quad (11)$$

Therefore, even with a generous choice of ΔU_\odot , etc., the data reject the possibility that the Sun has the DB98 value of \mathbf{v}_\odot . Reducing the widths ΔU_\odot , etc., of the priors on \mathbf{v}_\odot would strengthen the case against the DB98 value of \mathbf{v}_\odot .

The choice of $\Delta U_\odot \sim 100 \text{ km s}^{-1}$ is reasonably generous, and it is sensible to ask what value of ΔU_\odot , etc., would bring $p(\text{B09}|\text{data})/p(\mathbf{v}_\odot \text{ free}|\text{data})$ down to unity. In the case where the GDII rotation curve is used, it would require a reduction to a value $\Delta U_\odot \sim 30 \text{ km s}^{-1}$ – this is smaller than is reasonable given that the value for V_\odot found when it is allowed to vary is already $\sim 15 \text{ km s}^{-1}$ greater than the canonical DB98 value.

It is worth noting that the case for setting \mathbf{v}_\odot free from either the DB98 value or the B09 value is weakest when the best-motivated rotation curve is adopted – the GDII curve.

The lowest values of both v_0 and R_0 are found for the models with the DB98 value of \mathbf{v}_\odot , and \mathbf{v}_{SFR} set to zero. Both v_0 and R_0 take larger values for models with the B09 value of \mathbf{v}_\odot , and larger still for models with either \mathbf{v}_\odot or \mathbf{v}_{SFR} allowed to vary. The lowest values of v_0 and R_0 for the models in which the peculiar velocities are allowed to vary are 232 km s^{-1} and 7.7 kpc respectively.

Fig. 3 suggests a reason why the value of \mathbf{v}_\odot or \mathbf{v}_{SFR} in the model has such a large impact on the best fitting values of v_0 and R_0 . It shows the residual velocities of the

Table 1. Log likelihoods for best-fitting models with flat rotation curves ($\alpha = 0$), power law rotation curves ($\alpha \neq 0$) and rotation curves taken from GDII. The first 9 likelihoods are for models in which the sources are assumed to have no typical velocity – for the first 3 the value of \mathbf{v}_\odot is that found in DB98; the next 3 are for models in which \mathbf{v}_\odot is assumed to be that suggested by B09; and the next 3 are for models in which \mathbf{v}_\odot is allowed to vary freely; the final 3 are for cases in which \mathbf{v}_\odot is taken to be the DB98 value, and the mean source peculiar motion with respect to their local standard of rest, \mathbf{v}_{SFR} , is allowed to vary freely.

| | v_0 (km s ⁻¹) | R_0 (kpc) | α | U_\odot (km s ⁻¹) | V_\odot (km s ⁻¹) | W_\odot (km s ⁻¹) | Δ_v (km s ⁻¹) | v_0/R_0 (km s ⁻¹ kpc ⁻¹) | log(\mathcal{L}) |
|--------------------------------|--------------------------------|--------------------|-----------------------|------------------------------------|------------------------------------|------------------------------------|---|--|----------------------|
| DB98 | 200 ± 20 | 6.7 ± 0.5 | 0 | 10.0 | 5.2 | 7.2 | 10.0 ± 1.3 | 30.1 ± 1.7 | 26.8 |
| | 209 ± 26 | 6.9 ± 0.7 | 0.10 ± 0.16 | 10.0 | 5.2 | 7.2 | 10.0 ± 1.3 | 30.4 ± 1.7 | 27.1 |
| | 218 ± 20 | 7.1 ± 0.5 | GDII | 10.0 | 5.2 | 7.2 | 9.3 ± 1.2 | 30.8 ± 1.6 | 30.7 |
| B09 | 215 ± 19 | 7.0 ± 0.5 | 0 | 10.0 | 11.0 | 7.2 | 8.1 ± 1.1 | 30.5 ± 1.5 | 35.7 |
| | 228 ± 24 | 7.4 ± 0.6 | 0.15 ± 0.13 | 10.0 | 11.0 | 7.2 | 8.0 ± 1.1 | 30.8 ± 1.5 | 36.5 |
| | 235 ± 19 | 7.6 ± 0.5 | GDII | 10.0 | 11.0 | 7.2 | 7.6 ± 1.0 | 31.1 ± 1.5 | 38.9 |
| \mathbf{v}_\odot free | 232 ± 24 | 7.7 ± 0.6 | 0 | 8.1 ± 2.9 | 18.6 ± 2.4 | 9.7 ± 2.0 | 7.1 ± 1.0 | 30.0 ± 1.8 | 42.5 |
| | 258 ± 32 | 8.6 ± 0.9 | 0.27 ± 0.13 | 8.1 ± 2.8 | 19.5 ± 2.5 | 10.1 ± 2.0 | 7.1 ± 1.0 | 29.9 ± 1.7 | 45.4 |
| | 246 ± 24 | 8.1 ± 0.6 | GDII | 8.3 ± 2.8 | 16.5 ± 2.4 | 9.9 ± 2.0 | 7.0 ± 1.0 | 30.3 ± 1.8 | 43.5 |
| | v_0 | R_0 | α | $v_{R,\text{SFR}}$ | $v_{\phi,\text{SFR}}$ | $v_{z,\text{SFR}}$ | Δ_v | v_0/R_0 | log(\mathcal{L}) |
| \mathbf{v}_{SFR} free | 241 ± 24 | 7.7 ± 0.6 | 0 | 3.3 ± 2.8 | -12.9 ± 2.4 | 2.5 ± 2.0 | 7.0 ± 1.0 | 31.1 ± 1.7 | 42.9 |
| | 279 ± 33 | 8.9 ± 0.9 | 0.25 ± 0.12 | 2.0 ± 2.8 | -14.8 ± 2.5 | 3.0 ± 2.0 | 6.6 ± 1.0 | 31.5 ± 1.6 | 45.5 |
| | 259 ± 23 | 8.2 ± 0.6 | GDII | 2.5 ± 2.8 | -11.0 ± 2.4 | 2.8 ± 2.0 | 7.1 ± 1.0 | 31.6 ± 1.7 | 43.8 |
| v_0 (km s ⁻¹) | R_0 (kpc) | U_\odot | V_\odot | W_\odot | v_m | Δ_v | v_0/R_0 (km s ⁻¹ kpc ⁻¹) | log(\mathcal{L}) | |
| 233 ± 20 | 7.3 ± 0.5 | 10.0 | 5.2 | 7.2 | -8.1 ± 2.7 | 8.0 ± 1.1 | 31.6 ± 1.5 | 36.2 | |
| 247 ± 19 | 7.8 ± 0.4 | 10.0 | 11.0 | 7.2 | -6.2 ± 2.4 | 6.8 ± 0.9 | 31.4 ± 1.4 | 43.1 | |
| 259 ± 25 | 8.2 ± 0.5 | 10.7 ± 3.3 | 15.0 ± 2.7 | 10.0 ± 2.0 | -4.8 ± 2.9 | 6.5 ± 1.0 | 31.4 ± 1.9 | 46.0 | |
| v_0 (km s ⁻¹) | R_0 (kpc) | $v_{R,\text{SFR}}$ | $v_{\phi,\text{SFR}}$ | $v_{z,\text{SFR}}$ | v_m | Δ_v | v_0/R_0 (km s ⁻¹ kpc ⁻¹) | log(\mathcal{L}) | |
| 271 ± 25 | 8.2 ± 0.6 | 2.0 ± 3.1 | -9.7 ± 2.8 | -2.5 ± 2.2 | -5.8 ± 3.3 | 6.4 ± 1.1 | 32.9 ± 2.0 | 46.0 | |

Table 2. Similar to Table 1. This shows the best-fitting parameters (and corresponding log likelihoods) for models with a GDII rotation curve, and with the value v_m allowed to vary.

objects after the expected velocity is subtracted (ignoring the uncertainty in parallax). The objects that provide the strongest indication that some change in peculiar motion is required (indicated by open squares) are all relatively close to the Sun. Consequently, changes in R_0 and v_0 have a relatively small “lever arm” with which to bring the model closer to the data, with rather large changes required in order to have any significant impact on the expected values of the observables for those objects. The introduction of a new peculiar velocity (either of the sources or the Sun) allows the model to compensate for the significant discrepancy between the velocity of these objects and those expected from the rotation curve, without producing a major effect on the best-fitting values of R_0 and v_0 .

3.1 Maser line-of-sight velocities

Finally we consider models in which we allow for a systematic difference between the measured line-of-sight velocity of a maser and the line-of-sight velocity of the exciting star – such a difference would arise if masing occurred on the near side of an expanding shell around the star. We have done this for all the rotation curves described in this paper, but the results are sufficiently similar to one another that we only present (in Table 2) the results for the GDII rotation curve.

We again compare the different models by calculating the ratios of their evidences, using the prior for v_m uniform in a range of width $\Delta v_m = 20 \text{ km s}^{-1}$. We find

$$\frac{p(v_m = 0|\text{data})}{p(v_m \text{ free}|\text{data})} \simeq \begin{cases} 0.01 & \text{for DB98} \\ 0.06 & \text{B09} \\ 0.3 & \mathbf{v}_\odot \text{ free} \\ 0.3 & \mathbf{v}_{\text{SFR}} \text{ free} \end{cases} \quad (12)$$

so in each case the data support adding the extra free parameter.

If we accept this extra parameter in our models, we have to reconsider the evidence for a change in \mathbf{v}_\odot (or \mathbf{v}_{SFR}). The relevant ratios of evidences are:

$$\frac{p(\text{DB98}, v_m \text{ free}|\text{data})}{p(\text{B09}, v_m \text{ free}|\text{data})} \simeq 0.001, \quad (13)$$

$$\frac{p(\text{DB98}, v_m \text{ free}|\text{data})}{p(\mathbf{v}_\odot, v_m \text{ free}|\text{data})} \simeq 0.3, \quad (14)$$

$$\frac{p(\text{B09}, v_m \text{ free}|\text{data})}{p(\mathbf{v}_\odot, v_m \text{ free}|\text{data})} \simeq 220. \quad (15)$$

So the B09 value of \mathbf{v}_\odot is still favoured. Moreover, when \mathbf{v}_\odot is taken to be free, the likelihood still peaks at an even larger value of V than that of B09.

We note that the sources providing the strongest evidence that a non-zero value of v_m is needed are those ringed in the the bottom right plot of Fig. 3, all associated with the

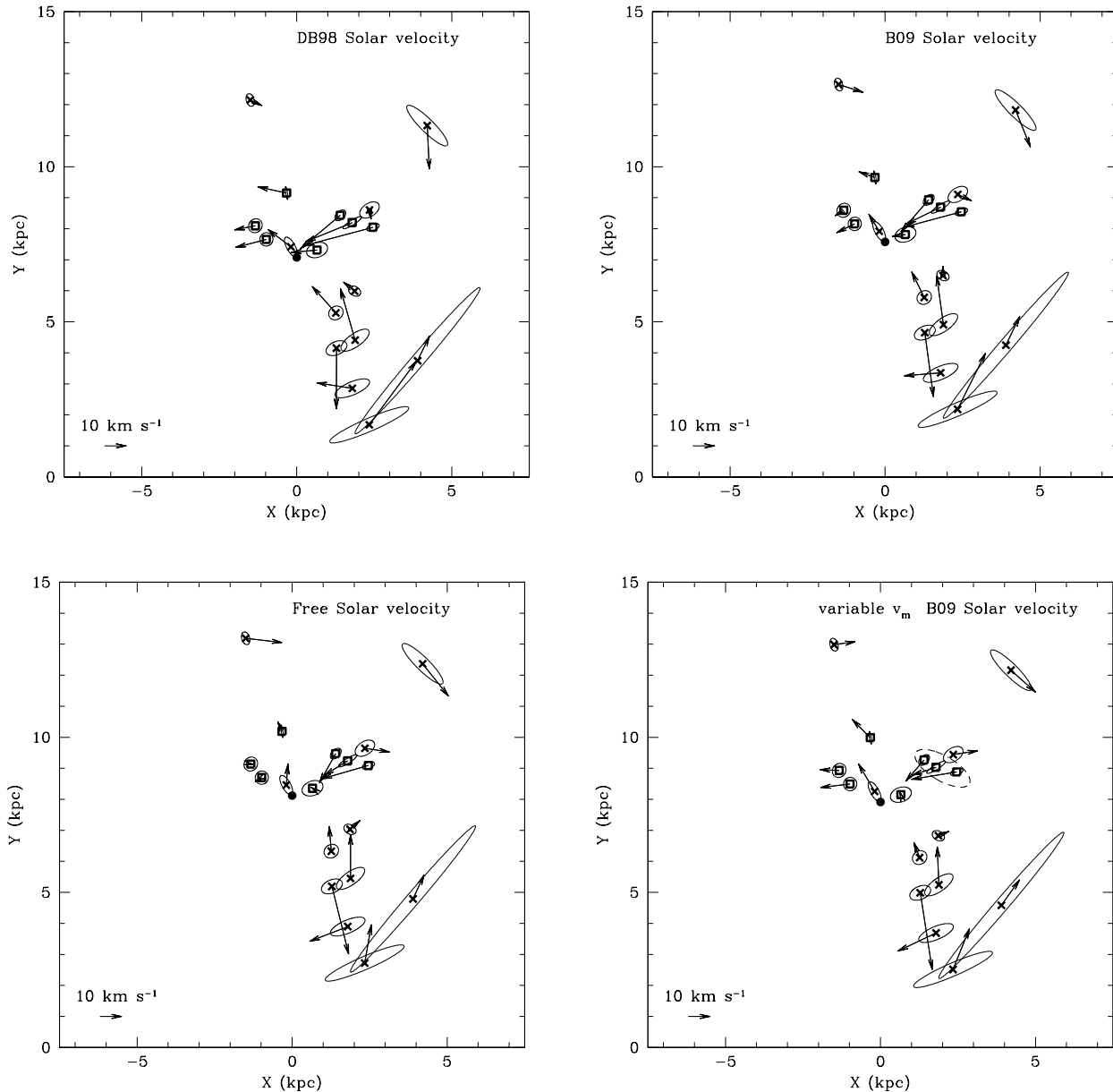


Figure 3. Residual velocities left after the best-fitting model velocities are subtracted, for models with GDII rotation curves and \mathbf{v}_\odot taking the DB98 value (top-left); the B09 value (top-right); or taken to be a free parameter (bottom-left). We also plot the residual velocities left after subtracting the best fitting model velocities for a model with the B09 \mathbf{v}_\odot value, and v_m taken to be a free parameter (bottom-right). *Open squares* correspond to the objects for which the likelihood improves most significantly between the best-fitting DB98 model and the best-fitting free Solar velocity one ($\Delta(\log \mathcal{L}_i) > 1$), and *crosses* to all other sources. The Sun is represented by a solid circle. The *solid lined ellipses* around each point are 1 σ measurement error ellipses, where the velocity error perpendicular to the line of sight in each case is due to a combination of the uncertainty in the proper motion and in the parallax. The uncertainty in the parallax also means that the residual velocities shown here are not an ideal illustration of the difference between the model and the data, because the peculiar motions can only be given for a chosen position (in this case the position corresponding to the quoted parallax). However this does provide a useful guide, especially for sources relatively close to the Sun, which have small position uncertainties. The *dashed ellipse* in the bottom-right plot is drawn around the three objects for which the likelihood improves most significantly when v_m is taken to be a free parameter ($\Delta(\log \mathcal{L}_i) > 1$ for B09 \mathbf{v}_\odot)

Perseus spiral arm (Reid et al. 2009). If we exclude these sources, the best fitting value of v_m is $\sim -3 \text{ km s}^{-1}$ for any assumption about \mathbf{v}_\odot we consider. This is approximately within the uncertainty on v_m , and if we considered only this subset of the data in equation (12), the evidence would

not support adding the extra free parameter v_m (though it should be noted that it is still a radial velocity *towards* the Sun). It is, therefore, possible that what we have modelled as an offset in the radial velocities of all observations is actually primarily due to a large peculiar velocity of the objects

in the Perseus arm, directed approximately in the direction of the Sun.

4 DISCUSSION

These results, and in particular the large variation in v_0 and R_0 depending on the other model parameters, makes it impossible to constrain tightly either v_0 or R_0 from these data – the smallest best-fitting values of these parameters are, respectively, 40 per cent and 33 per cent smaller than the largest best-fitting values. The choice of rotation curve has a significant impact, and we do not investigate all possible rotation curves. It is worth noting that our two most favoured models in Table 1 (according to Bayesian evidence, so somewhat dependent on our choice of priors) have best-fitting values of v_0 that differ by 30 km s^{-1} and of R_0 that differ by 1 kpc from one another (the models are those with B09 \mathbf{v}_\odot + GD rotation curve and free \mathbf{v}_\odot + power-law rotation curve, respectively).

However, for all but one of our models the best fitting v_0/R_0 lie in the narrow range $(29.8 - 31.5) \text{ km s}^{-1} \text{ kpc}^{-1}$, with typical uncertainties $\sim 1.5 \text{ km s}^{-1} \text{ kpc}^{-1}$. This corresponds to best fitting $(v_0 + V_\odot)/R_0$ in the range $(30.9 - 32.5) \text{ km s}^{-1} \text{ kpc}^{-1}$ (again, depending on the model), with similar uncertainties. These values are slightly larger than the value of $(v_0 + V_\odot)/R_0 = 30.2 \pm 0.2 \text{ km s}^{-1} \text{ kpc}^{-1}$ found from the proper motion of Sgr A* (Reid & Brunthaler 2004), but consistent to within (less than) twice the uncertainties on our values.

If we allow for a bias in the maser radial velocities with respect to the Sun by allowing the parameter v_m to take a non-zero value in equation (4), this does improve the fit. However we have seen that this is primarily due to a group of maser sources in the Perseus spiral arm, so the cause may be a large peculiar motion in that part of the Galaxy. Even if the bias in measured radial velocity is real, it does not affect the result: (i) that in different models these data are fit best by very different values of v_0 and R_0 ; (ii) that the DB98 \mathbf{v}_\odot is rejected by these data, and (iii) that the B09 \mathbf{v}_\odot is favoured over making \mathbf{v}_\odot a free parameter.

Reid et al. (2009) focused on the idea that these data show that the HMSFRs are orbiting the Galaxy with a velocity that lags the circular speed by $-v_{\phi, \text{SFR}} \sim 15 \text{ km s}^{-1}$. Our analysis of similar models shows that the data are fit better by a slightly smaller offset of $(11 - 14.8) \text{ km s}^{-1}$ to the circular speed. We have also shown that an equivalent fit to the data can be obtained by instead increasing to $\sim 17 \text{ km s}^{-1}$ the amount V_\odot by which the Sun is assumed to circulate faster than the circular speed. In fact, the sources that provide the strongest statistical support for $v_{\phi, \text{SFR}} \sim -15 \text{ km s}^{-1}$ are found near the Sun (Fig. 3), so a change in \mathbf{v}_\odot has a very similar effect to a change in \mathbf{v}_{SFR} . More maser data at different Galactic azimuths could break this degeneracy, as well as reducing the correlation between the values of v_0 and R_0 seen in Fig. 2.

If the proposal of Reid et al. (2009) that $v_{\phi, \text{SFR}} \simeq -15 \text{ km s}^{-1}$ were correct, the HMSFRs would all have to be close to apocentre. Since the lifetime of an HMSFR is short compared to a typical epicycle period and spiral structure must play a significant role in their formation, it is not inherently implausible that the maser stars are all close to

apocentre. However, two arguments make it unlikely that the maser stars are on orbits as eccentric as is implied by a 15 km s^{-1} offset from circular motion at apocentre.

First, non-axisymmetric structure in the Galaxy’s potential modulates the tangential velocity of gas by only $\sim 7 \text{ km s}^{-1}$ (e.g. Binney & Merrifield 1998, §9.2.3), so the HMSFRs would be moving with a peculiar velocity significantly higher than the gas from which they formed. Second, by GDII (equation 3.100), a quarter of an epicycle period later the U velocities of these stars would be $(2\Omega/\kappa)15 \text{ km s}^{-1} \simeq 22 \text{ km s}^{-1}$, where Ω and κ are the circular and radial frequencies at the star’s location. Hence the radial velocity dispersion of a population of such stars would be at least $\sim 22/\sqrt{2} \simeq 15 \text{ km s}^{-1}$. The velocity dispersion of stars observed locally increases with age on account of heating by irregularities in the Galaxy’s gravitational field (e.g. GDII §10.4.1) and the velocity dispersion of the bluer stars in the Hipparcos catalogue is $\sim 10 \text{ km s}^{-1}$ (Aumer & Binney 2009) rather than 15 km s^{-1} . Thus the conjecture of Reid et al. (2009) not only requires the masing stars to be confined to apocentre but also requires them to have more eccentric orbits than the generality of young stars. Recognising this problem, Reid et al. suggested that the orbits of these stars became more circular early in their lives. However, any random scattering process spreads stars more widely in phase space and therefore increase the mean eccentricity of the masing stars. Only a dissipative process could increase the phase-space density of these stars by moving them to more circular orbits, and no such process is known.

If the B09 value of V_\odot is correct, the lag to circular motion required to optimise the fit to the data is so small ($\sim 5 \text{ km s}^{-1}$) that the above objections to the proposal that HMSFR systematically lag rotation become moot. However, the formalism of Bayesian inference says that when the B09 value of V_\odot is accepted, there is no convincing evidence for a systematic lag of the HMSFR.

Throughout this paper we have proceeded under the assumption that the velocity of the LSR is the same thing as the circular velocity at R_0 . It is worth noting that this is not necessarily the case. The LSR is defined to be the velocity of a closed orbit as it passes the current Solar position, which will only be a circular orbit if the Galactic potential is axisymmetric. Therefore the velocity of the LSR may be offset from the circular velocity curve. However (much like the possibility of a systematic lag of the HMSFR) we should note that if we accept the B09 value of V_\odot , there is no convincing evidence for this offset.

We conclude that these data provide a compelling case for revising V_\odot upward. Our Bayesian analysis (equation 10) supports the revision upwards of V_\odot to 11 km s^{-1} suggested by B09 on the basis of modelling predominantly old disc stars with relatively large random velocities. It should, however, be recognised that an even better fit to *these* data comes from somewhat larger upward revisions to $V_\odot \sim 16 - 20 \text{ km s}^{-1}$.

5 CONCLUSIONS

We have reanalysed observations of HMSFRs reported in Reid et al. (2009) using a maximum-likelihood approach to

exploit fully the data, in an effort to determine the values of R_0 , the Galactocentric radius of the Sun, and v_0 , the circular velocity of the LSR. We have found that the best-fitting values, considered separately, are strongly dependent on the Galaxy model used to interpret the data, but that the ratio v_0/R_0 is consistently found to lie in the range $29.8 - 31.5 \text{ km s}^{-1} \text{ kpc}^{-1}$.

We have also used these data to explore the value of the Sun's peculiar velocity \mathbf{v}_\odot , in light of the recent argument of B09 that the canonical DB98 value is incorrect. We find that these data support the conclusion that V_\odot is significantly higher than the DB98 value. By a small but significant margin, the data prefer models with the B09 revision of V_\odot to $\sim 11 \text{ km s}^{-1}$ over models in which \mathbf{v}_\odot is left as a free parameter (equation 10). The best-fitting models have U_\odot and W_\odot near to the DB98 values, and the even larger value of $V_\odot \sim 16 - 20 \text{ km s}^{-1}$.

Reid et al. (2009) suggested that HMSFRs significantly lag circular rotation. We have investigated the possibility that the HMSFRs have a typical peculiar velocity \mathbf{v}_{SFR} and find that the models only constrain the velocity difference $\mathbf{v}_{\text{SFR}} - \mathbf{v}_\odot$. We have argued that models in which the HMSFRs have large peculiar velocities in the opposite direction to Galactic rotation are neither needed nor plausible.

This work, in conjunction with B09, casts severe doubt on the accuracy of the widely used DB98 value for V_\odot . This must be a concern for anyone interested in the dynamics within the Milky Way because velocities are inevitably measured with respect to the Sun. Both observations of more masers and the development of a detailed dynamical model of the Galaxy's spiral structure would contribute to establishing more securely what the true value of V_\odot is.

ACKNOWLEDGMENTS

We thank John Magorrian and the other members of the Oxford dynamics group for valuable discussions. PJM is supported by a grant from the Science and Technology Facilities Council.

NOTE ADDED AFTER ACCEPTANCE

After this paper was accepted for publication, Rygl et al. (2009) presented similar observations of maser sources. Incorporating these observations in our analysis does not materially affect our conclusions.

REFERENCES

- Aumer M., Binney J. J., 2009, MNRAS, 397, 1286
 Binney J., Merrifield M., 1998, Galactic astronomy. Princeton University Press
 Binney J., Tremaine S., 2008, Galactic Dynamics: Second Edition. Princeton University Press
 Binney J. J., 2009, MNRAS, accepted, arXiv:0910.1512 (B09)
 Chatterjee P., Hernquist L., Loeb A., 2002, ApJ, 572, 371
 Dehnen W., Binney J. J., 1998, MNRAS, 298, 387
 Gelman A., Rubin D. B., 1992, Statistical Science, 7, 457
 Ghez A. M., Salim S., Weinberg N. N., Lu J. R., Do T., Dunn J. K., Matthews K., Morris M. R., Yelda S., Becklin E. E., Kremenek T., Milosavljevic M., Naiman J., 2008, ApJ, 689, 1044
 Gillessen S., Eisenhauer F., Trippe S., Alexander T., Genzel R., Martins F., Ott T., 2009, ApJ, 692, 1075
 Heavens A., 2009, arXiv: 0906.0664
 Koposov S. E., Rix H.-W., Hogg D. W., 2009, ApJ, submitted, (arXiv: 0907.1085)
 Metropolis N., Rosenbluth A. W., Rosenbluth M. N., Teller A. H., Teller E., 1953, Journal of Chemical Physics, 21, 10871092
 Reid M. J., 1993, AnnRA&A, 31, 345
 Reid M. J., Brunthaler A., 2004, ApJ, 616, 872
 Reid M. J., Menten K. M., Zheng X. W., Brunthaler A., Moscadelli L., Xu Y., Zhang B., Sato M., Honma M., Hirota T., Hachisuka K., Choi Y. K., Moellenbrock G. A., Bartkiewicz A., 2009, ApJ, 700, 137
 Rygl K. L. J., Brunthaler A., Reid M. J., Menten K. M., van Langevelde H. J., Xu Y., 2009, A&A, accepted (arXiv:0910.0150)